Control of Permafrost and Seasonal Frost on Stream and Groundwater Interactions in Alpine Catchment, Northeastern Tibet Plateau, China

Rui Ma[1], Mengyan Ge[1], Ziyong Sun[1], and Qixin Chang[1]

[1]China University of Geosciences - Wuhan

November 24, 2022

Abstract

The role of groundwater in maintaining streamflow in the alpine area with distribution of permafrost and seasonal frost is a poorly studied topic of considerable interest. The stream and groundwater interactions and groundwater contributions to the Heihe River were investigated during this study in a representative subcatchment in the headwater region of the Heihe River Basin, the northeastern Qinghai-Tibet Plateau of China. The hydraulic, chemical and isotopic data as well as Bayesian mixing model results show that groundwater-stream water interactions were both spatially and temporally variable. The tributaries were primarily recharged by springs within the permafrost zone during the frozen period when the water source and sediments were frozen and the groundwater discharged to the mainstream within the seasonal frost zone to maintain the streamflow. The groundwater contribution to mainstream discharge decreased from 95% during the frozen period to 80-90% in the thawing period due to the inflow from tributaries. However, the stream and groundwater interactions vary several times along altitude during the thawed period from June to early September, due to the increased glacial/snow meltwater volume, deepened active layer, and melted seasonal frost. Groundwater contribution decreased to ~40-60% of the mainstream discharge during the thawed period because tributary streams contribution largely increased. As shown by ~70-90% contribution from groundwater to the mainstream discharge, the mainstream flow mainly sourced from the release of groundwater in aquifers in the freeze-back period. These data indicate that the variations in groundwater-surface water interactions were largely influenced by the distribution and freeze-thaw cycle of permafrost and seasonal frost. The importance of groundwater storage in maintaining streamflow in the Heihe headwater region was highlighted by this study.

Hosted file

`essoar.10504313.1.docx` available at https://authorea.com/users/543465/articles/603106-control-of-permafrost-and-seasonal-frost-on-stream-and-groundwater-interactions-in-alpine-catchment-northeastern-tibet-plateau-china

Control of Permafrost and Seasonal Frost on Stream and Groundwater Interactions in Alpine Catchment, Northeastern Tibet Plateau, China

Rui Ma*, Mengyan Ge, Ziyong Sun, and Qixin Chang

School of Environmental Studies and State Key Laboratory of Biogeology and Environmental Geology, China University of Geosciences, Wuhan, China

Corresponding author: Rui Ma (rma@cug.edu.cn)

Abstract

The role of groundwater in maintaining streamflow in the alpine area with distribution of permafrost and seasonal frost is a poorly studied topic of considerable interest. The stream and groundwater interactions and groundwater contributions to the Heihe River were investigated during this study in a representative subcatchment in the headwater region of the Heihe River Basin, the northeastern Qinghai-Tibet Plateau of China. The hydraulic, chemical and isotopic data as well as Bayesian mixing model results show that groundwater-stream water interactions were both spatially and temporally variable. The tributaries were primarily recharged by springs within the permafrost zone during the frozen period when the water source and sediments were frozen and the groundwater discharged to the mainstream within the seasonal frost zone to maintain the streamflow. The groundwater contribution to mainstream discharge decreased from 95% during the frozen period to 80-90% in the thawing period due to the inflow from tributaries. However, the stream and groundwater interactions vary several times along altitude during the thawed period from June to early September, due to the increased glacial/snow meltwater volume, deepened active layer, and melted seasonal frost. Groundwater contribution decreased to ~40-60% of the mainstream discharge during the thawed period because tributary streams contribution largely increased. As shown by ~70-90% contribution from groundwater to the mainstream discharge, the mainstream flow mainly sourced from the release of groundwater in aquifers in the freeze-back period. These data indicate that the variations in groundwater-surface water interactions were largely influenced by the distribution and freeze-thaw cycle of permafrost and seasonal frost. The importance of groundwater storage in maintaining streamflow in the Heihe headwater region

was highlighted by this study.

Keywords: alpine catchment; stream and groundwater interactions; permafrost; seasonal frost zone; freeze-thaw process

1 Introduction

Many large rivers, such as the Yukon River of Alaska, USA, the Lena and Kolyma rivers in Siberia, Russia, and the Yangtze, Yellow, Tarim and Heihe rivers in China, originate within the cryosphere, where water exists in surficial geological materials in solid form (often as permafrost). During the past decade, there has been a growing interest in the contribution of groundwater to these types of river systems. This increased interest stems largely from the observed changes in the flux of such rivers as the Yukon in Canada (Dornblaser and Striegl 2007, 2009; Schuster et al. 2011; O'Donnell et al. 2012), and the Ob', Yenisey and Lena rivers in Russia (Frey et al. 2007; Smith et al. 2007), which may reflect the melting of permafrost in response to climate change (Garey et al., 2013). While groundwater discharge to these rivers is readily apparent indicated by the river icings and the occurrence of open water throughout the winter, the subsurface groundwater flow paths and the contribution of groundwater to the total discharge remain uncertain (Woo and Marsh, 2005).

The existing studies on groundwater and surface water interaction in cryosphere focused mainly in arctic-subarctic area, where is characterized by low temperature, continuous distribution of thick layer permafrost with surface runoff mainly occurring in spring freshet period, and the active layer being deepest in summer (Chang et al., 2018). In comparison, the middle and low latitude alpine catchments in the Qinghai-Tibet Plateau are featured by the variable terrain and landforms as well as large local altitude differences, and often underlie by co-existed continuous permafrost, discontinuous permafrost, and seasonal frost (Cheng and Jin, 2013). In this area, the majority of annual precipitation falls and glacier melt mainly occurs during summer, when the active layer also thaws to reach the maximum depth within one year (Lu et al., 2004). The characteristics of permafrost and seasonal frost distribution and hydrological conditions may lead to a complex flow path regime and frequent interactions between groundwater and surface water, further influencing the catchment discharge pattern (Woo, 2012). However, few studies have been conducted to investigate the controls of the complex distribution pattern and freeze-thaw processes of permafrost and seasonal frost on surface water and groundwater interaction in the alpine area.

Several methods have been widely used to investigate the interactions between surface water and groundwater, including the use of potentiometric data, groundwater temperature, and various types of isotopic (O, H, Sr) and geochemical (e.g. cation ratio) data (Mondal et al., 2010 and references therein). Hydrogeological data in remote cryosphere were often lacking due to limited infrastructure. Thus, geochemical and isotopic methods are becoming an increasingly important approach to the study of groundwater and surface-water interactions (Rautio and Korkka-Niemi, 2015). For example, Anderson et al. (2013) combined the analysis of remotely sensed imagery with lake water oxygen and hydrogen isotopic compositions to identify the existence and cause of lake area changes within Yukon Flats, a region of discontinuous permafrost in north-central Alaska. The isotope data indicated that ~5% of the water volume within the studied lakes was derived from the melting of snow and/or permafrost. Rautio and Korkka-Niemi (2015) also employed a combination of chemical and isotopic tracers to assess groundwater and surface water interactions within a boreal lake catchment in Finland. The concentrations and isotopic ratios of dissolved inorganic carbon (DIC) have also been jointly used to determine groundwater and surface water interactions (Utting et al., 2013).

The mixing models are often employed when using tracers to quantify the contribution of groundwater to surface water. The simple linear mixing model has been widely used to determine the contribution fraction of each water source to a river given the assumption that there is limited variability in the geochemical composition of the source waters (e.g., Brassard et al., 2000). However, such model has been proven to be problematic, in part because the geochemical or isotopic compositions of source waters are often similar or may even overlap, significantly increasing uncertainty in the modeling results (Davis et al., 2015). Thus, Bayesian mixing model, which considers the uncertainties associated with the measured tracer concentrations in waters and their affecting factors, has been more widely applied to separate different sources in recent years (Cable et al., 2011; Arendt et al., 2015; Davis et al., 2015). For example, Cable et al. (2011) applied the Bayesian modeling technique with H and O isotope data to estimate the fractional contribution of glacier meltwater to Dinwoody Creek in the Wind River Range of Wyoming on a bi-weekly and seasonal time scale over for two years.

Heihe River, the second largest inland river in China, serves as an important water resource for domestic, agricultural and industrial needs in the Qinghai, Gansu and Inner Mongolia provinces of northwestern China (Wei et al., 2018). The headwater region of the Heihe River is located in the Qilian Mountains, which is covered by continuous and discontinuous permafrost and seasonal frost. Previous studies in the area focused on the hydrological processes of surface water (Jia et al., 2009; Wang et al., 2018; Gao et al., 2018) and the contribution of glacier and snow meltwater to river discharge (Li et al., 2014; Chang et al., 2018). The numerical models were developed to predict the effect of climate change on groundwater discharge to river (Evans et al., 2015). However, the model oversimplified the field condition and has a large uncertainty, and the surface water and groundwater interactions, including the contribution of groundwater to streamflow, remain unquantified based on the field site configuration.

The objective of this study is to improve our understanding of the groundwater and surface water interactions and quantify the contributions of groundwaters via different flow paths to the Hulugou stream, a representative tributary of the Heihe River. The data of hydraulics, geochemistry and naturally occurring isotopic tracers as well as the Bayesian mixing model were employed to identify different flow paths and estimate the relative contributions of potential water sources to the stream discharge. Inherent in the study is an assessment of the controls that the distribution and freeze-thaw processes of permafrost and seasonal frost exert on groundwater flow and its discharge to the stream.

2 Study site and background

The Hulugou catchment (located between 38°12'14"N-38°16'23"N latitude and 99°50'37"E-99°53'54"E longitude, Fig. 1) is an alpine catchment within the Qilian Mountains that rise along the northeast border of the Qinghai-Tibetan Plateau. The catchment possesses a drainage area of 23.1 km^2 and represents one of many headwater tributaries of the Heihe

River (Fig. 1). The elevation of the Hulugou catchment ranges from 2960 m a.s.l. to 4820 m a.s.l., and gradually decreases from south to north.

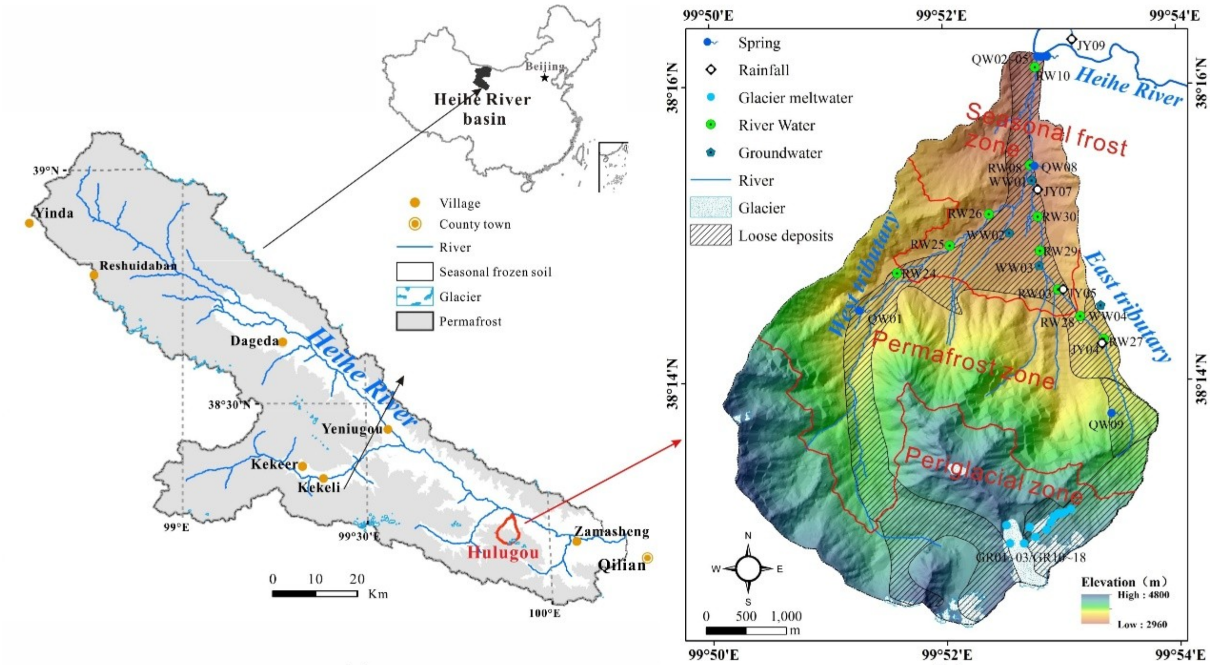

(a) (b)

Fig. 1. (a) Location of the headwater region of Heihe River (a), and (b) Hulugou Catchment study area showing sampling sites.

The catchment is characterized by a continental climate. Mean annual precipitation is 400 mm at low altitudes and increases to 600 mm at higher altitudes; 70% of the annual precipitation occurs during July–September (Chen et al., 2014a). Open water evaporation ranges from 376 to 650 mm/year. The mean annual temperature decreases from approximately 3.1°C at 3000 m a.s.l. to −4.0°C at 4200 m a.s.l., whereas the average annual temperature throughout the catchment is −3.9°C (Chen et al., 2014a). Variations in daily precipitation, stream discharge and temperature in 2014 to 2015 are shown in Fig. 2, which can be accessed at the WestDC database (http:// westdc.westgis.ac.cn/).

The area above 4200 m is mostly covered by five mountain glaciers (total area 0.827 km^2 in 2011) and seasonal snow, which in combination accounts for 8.4% of the total Hulugou catchment area. This area provides the majority of the water resources in the catchment, most of which are derived from ice and snow. The glaciers are included in the headwater conservation zone of the Heihe River (Liu and Chen, 2016; Li et al., 2014). The catchment has complicated terrain, but in general, is characterized by a systematic change with decreasing elevation from permafrost area with glacial and periglacial features to seasonal frost area with fluvioglacial features in a piedmont sloping plain. The south part of the study area consists of bedrock outcrops, whereas the northern part is composed of fluvioglacial fan(s).

Three important types of depositional units that serve as aquifers have been identified in Hulugou catchment, i.e., pro-glacial moraine and talus deposits, moraine and fluvioglacial deposits on planation surface, and fluvioglacial and moraine deposits in piedmont plain (Chang et al., 2018). The piedmont plain in the Hulugou catchment is composed of several partially superimposed fluvioglacial fans. The thick (20−50 m) deposits composed of poorly sorted, subangular, mud-bearing pebble gravels in the plain provide favorable aquifers for groundwater storing and transmission (Chang et al., 2018; Ma et al., 2017).

The permafrost is located at elevations higher than 3500 m a.s.l. (Wang et al., 2017), which serves as an aquitard in the area. The active layer is ~2 m thick and the underlying perennial frozen layer is ~20 m thick in the permafrost zone (Ma et al., 2017). The groundwater in the high mountains mainly occurred as suprapermafrost groundwater, while in the moraine and fluvioglacial deposits on the planation surfaces, suprapermafrost, intrapermafrost and subpermafrost groundwater co-occurred. The exchange between suprapermafrost and subpermafrost occurred since the permafrost distributes discontinuously (Ma et al., 2017). Springs or seeps were common at the upper slopes of the hills whose top was a planation surface with thick deposits.

The seasonal frost is located at elevations below 3500 m a.s.l. The seasonally frozen depth was about 2~3 m (Ma et al., 2017). Groundwater in the seasonal frost area primarily occurred in the fluvioglacial fan(s), as well as in the scree deposits of the mountains and the slope deposits of the hills. The deposits in the seasonal frost area mainly consist of sandy gravels which are highly permeable and groundwater flow directions generally correspond to the local topography. Thus, regional groundwater flow is oriented from the higher elevations in the south toward the lower elevations in the north and converges near the mouth of the catchment. Weathered sandstone was found at 22 m depth at the head of the alluvial plain (Ma et al., 2017).

The Hulugou stream is formed by the confluence of two large tributaries that are referred to as the east and west tributary. Both tributaries originate from glacial/snowmelt, progressively flow downstream through the glacial-periglacial area, permafrost area, and seasonal frost area, and converge at the elevation of 3400 m a.s.l. (Fig. 1). The east tributary is a seasonal stream, which is normally dry from November to May when the west tributary still has a small flux. From June to August the flow in both tributaries greatly increases (Fig. 2; Data from the WestDC database, http://westdc.westgis.ac.cn). The mainstream flow at the catchment outlet, i.e., the Hulugou stream discharge, exhibits the seasonal change (Data from the WestDC database, http://westdc.westgis.ac.cn). It increases suddenly in May, reaching its maximum value in July, then begins to decrease in October, and only remains a small value throughout the winter and early spring. The shallow soil in the seasonal frost area is completely frozen from December to March (frozen period), thawing from April to May (thawing period), completely thawed from June to early September (thawed period), and freezing back in late September to November (freeze-back period) (Fig. 2; Date from the WestDC database, http://westdc.westgis.ac.cn). The ground temperature in the active layer in the permafrost area also exhibits a similar dynamic change pattern (Ma et al., 2017). In this study, the period from December to April was referred to as a cold season, and that from June to September was referred to as a warm season.

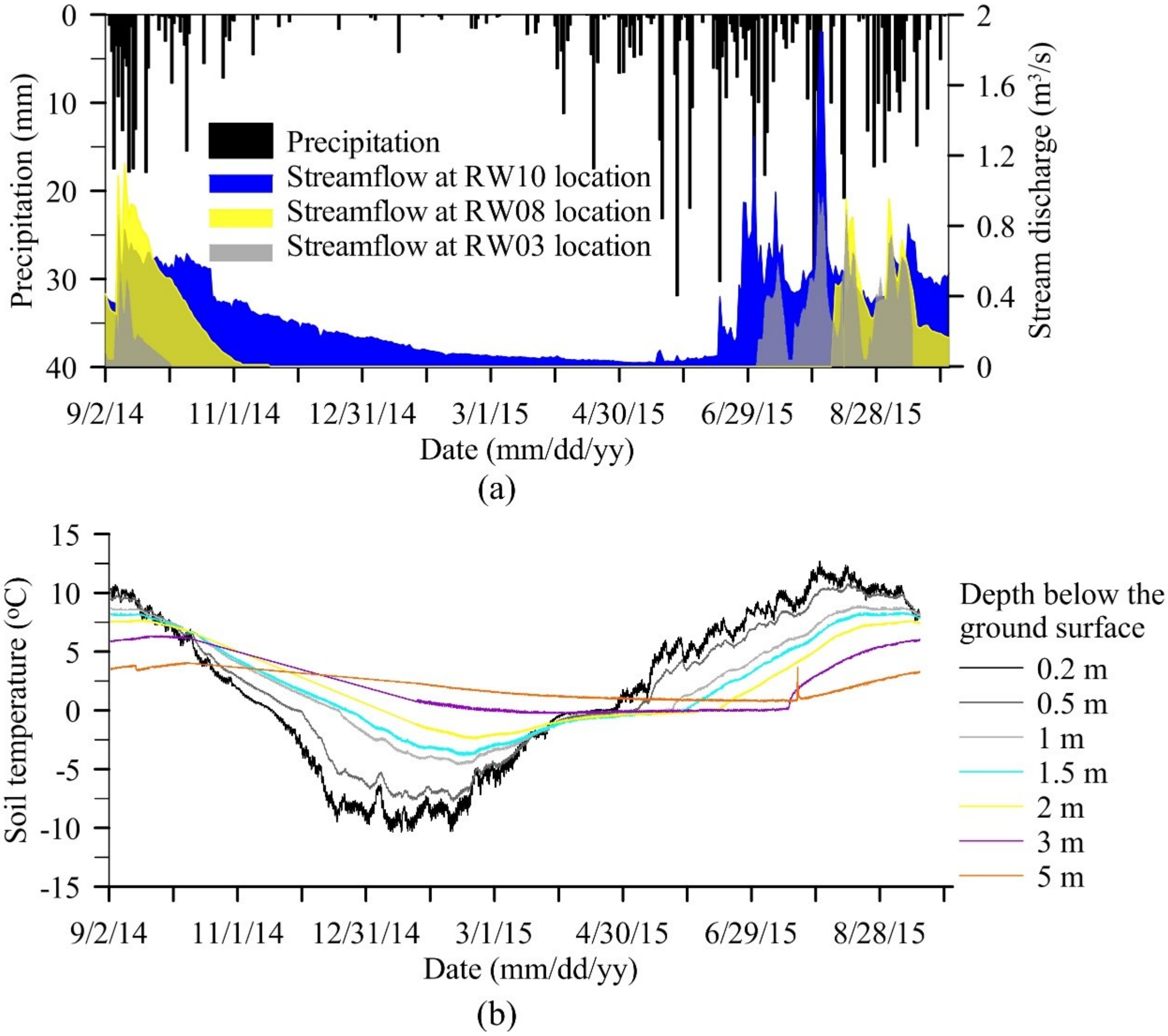

Fig. 2. (a) Precipitation recorded at an elevation of 3649 masl (black line); Hulugou streamflow (m^3/s) at different locations shown in Figure 1. (b) Soil temperature shown for various depths below the ground surface at an elevation of 3500 m within the Hulugou Catchment from September 2014 to September 2015.

3 Materials and methods

3.1. Groundwater monitoring

Three nested sets of wells (numbered WW01, WW02 and WW03) are located in the fluvioglacial fan(s) characterized by seasonal frost (Fig. 1). Each nested well set includes four depth-specific wells, which are screened at depths of 5 m, 10 m, 15 (or 20) m and 25 (or 30) m below the ground surface, respectively. One nested well set (WW04) is situated in the permafrost area as shown in Fig. 1. Individual wells at this site are screened at depths of 1.5 m, 12 m and 24.3 m below the ground surface, respectively.

The groundwater tables in each well were monitored using pressure transducers (a HOBO U20-001-02 water level logger; Onset, Bourne, MA, USA). Atmospheric pressure was simultaneously measured using a barometric pressure sensor (S-BPB-CM50; Onset, Bourne, MA, USA). These atmospheric data allowed groundwater tables to be corrected for changes in atmospheric pressure. The data loggers recorded water tables at 15-minute intervals, which was consistent with data collected by temperature probes.

3.2. Water sampling and analysis

Water samples were collected to analyze the concentrations of major ion, minor element Sr and Si, and dissolved organic carbon (DOC) and dissolved inorganic carbon (DIC) and the stable hydrogen (D) and oxygen (^{18}O) isotope compositions. The monitoring program included 12 regularly sampled sites for river water, 16 sites for groundwater, and 3 regularly sites for rain (Fig. 1). In addition to these regularly sampled sites, 28 sites were sampled for glacial/snow meltwater from the periglacial area, soil water or groundwater.

Samples of precipitation were collected weekly at elevations of 2960 m a.s.l., 3160 m a.s.l., 3360 m a.s.l., 3560 m a.s.l. and 4160 m a.s.l from 2011 to 2016. Springs and well waters from each nested well set (i.e., adjacent wells screened at different depths) were collected bi-weekly from 2012 to 2016, and from 2014 to 2016, respectively. Stream waters from the tributaries and mainstream were collected weekly from 2012 to 2016. In order to collect glacier/snow meltwater from beneath the snowpack, waters were collected seasonally from 2012 to 2015 at an elevation of 4680 m during the ablation period from small steams (4540 m a.s.l) on the glacier surface, and from waters located along the glacier front (4340 m a.s.l).

Groundwaters were sampled using a peristaltic pump after purging at least 2 well-volumes from the wells. Seven subsets of samples were collected from each site and filtered into polyethylene bottles that had been pre-washed with de-ionized water. There was no headspace when bottles were sealed for collecting samples for D and ^{18}O isotope analyses. Filtering was conducted in the field using 0.22 μm membranes. During groundwater sampling, physiochemical parameters of pH, electric conductivity, temperature and dissolved oxygen (DO) concentration were measured in situ using a portable Hatch water quality probe and a pH meter (HACH HQ40d). The equipment was calibrated for pH and DO measuring daily. Alkalinity was titrated in the field with the Gran method.

Samples for cation and minor element analysis were acidified with ultrapure HNO_3 to pH=2. The water samples were subsequently transported to the laboratory and analyzed for major and minor ions. Major anions (SO_4^{2-}, Cl^-, NO_3^-) were analyzed using ion chromatography (Dionex, model DX-120), whereas cations (Ca^{2+}, Mg^{2+}, K^+, Na^+) and Si and Sr were determined by ICP-AES (IRIS INTRE II XSP). All samples were analyzed within two weeks of sample collection.

An ultra-high precision isotopic water analyzer (L2130-I, Picarro, USA) was used to measure ^{18}O and ^{2}H compositions at the Laboratory of Basin Hydrology and Wetland Eco-restoration, China University of Geosciences (Wuhan). ^{18}O and ^{2}H compositions were expressed in δ per milliliter relative to the V-SMOW (Vienna Standard Mean Ocean Water), with analytical precision of 0.025‰ and 0.1‰, respectively. Analyses for DOC and DIC were performed by an Aurora 1030W TOC analyzer by means of a wet chemistry method, whose precision was 50 ppb. Mean values, standard deviations (± SD) and the number of samples for chemical concentrations and H and O isotopic compositions in different types of water are presented in Table 1.

3.3. Bayesian mixing model

To quantify the contributions of different water sources to the mainstream flow and their variations throughout the year, a Bayesian Monte Carlo (BMC) isotope mixing model developed by Arendt et al. (2015) was adopted by this study and the model can be written as follows:

$$p(f_i) \propto p'(f_i \wedge I_i) L(o_j \vee f_i \wedge I_i) \quad (1)$$

where f_i are the fractional contributions, o_j are the isotopic measurements, I_i are the isotopic compositions of the end-member components, $p(f_i)$ and $p'(f_i \wedge I_i)$ are the prior and posterior probability density functions (PDF), respectively, and $L(o_j \vee f_i \wedge I_i)$ is a data likelihood function. Bayesian estimation tests the statistical likelihood of the calculated isotopic values against the observations and then converts the prior PDF to a posterior PDF.

The sum of the fractions from each source to the mixture is constrained to equal 1. Gaussian and uncorrelated uncertainties on the measured isotopic compositions were assumed in the calculation. The data likelihood function is presented as follows (Arendt et al., 2015):

$$L(o_j \vee f_i \wedge I_i) \propto \prod_j \exp\left[\frac{(o_j^p - o_j)^2}{2\sigma_j^2}\right] \quad (2)$$

where σ_j are the uncertainties on the isotopic measurements and o_j^p are the isotopic values predicted by a test model of f_i and realization of I_i.

A straightforward Monte Carlo sampling scheme was adopted for model fitting. This scheme remained the selected samples of the prior as those of the posterior proportional to the likelihood based on the misfit between predictions and observations.

4. Results

4.1. Groundwater table depth

The groundwater table was deeper than the screen depth of 30 m at well WW02 in the middle of the piedmont plain and thus was not monitored during the study period. The groundwater depth over time at nested wells sets WW01, WW03 and WW04 are shown in Fig. 3. The groundwater depth in the 20 m and 30 m wells at the top of the piedmont plain

(WW03) changed from 13 m to 18 m below ground from June to September and declined to 22−23 m from November to next May. The groundwater table depth in the 10 m, 15 m and 25 m wells at the base of piedmont plain (WW01) was between 4 m and 6 m below ground from June to November but dropped to ~16−22 m below ground from January to May. The water table depth in the suprapermafrost groundwater (WW04) was close to the ground surface from June to September and decreased to 1.5 m below ground from October to December, while it in the subpermafrost groundwater varied between 20.3 and 23.5 m below ground.

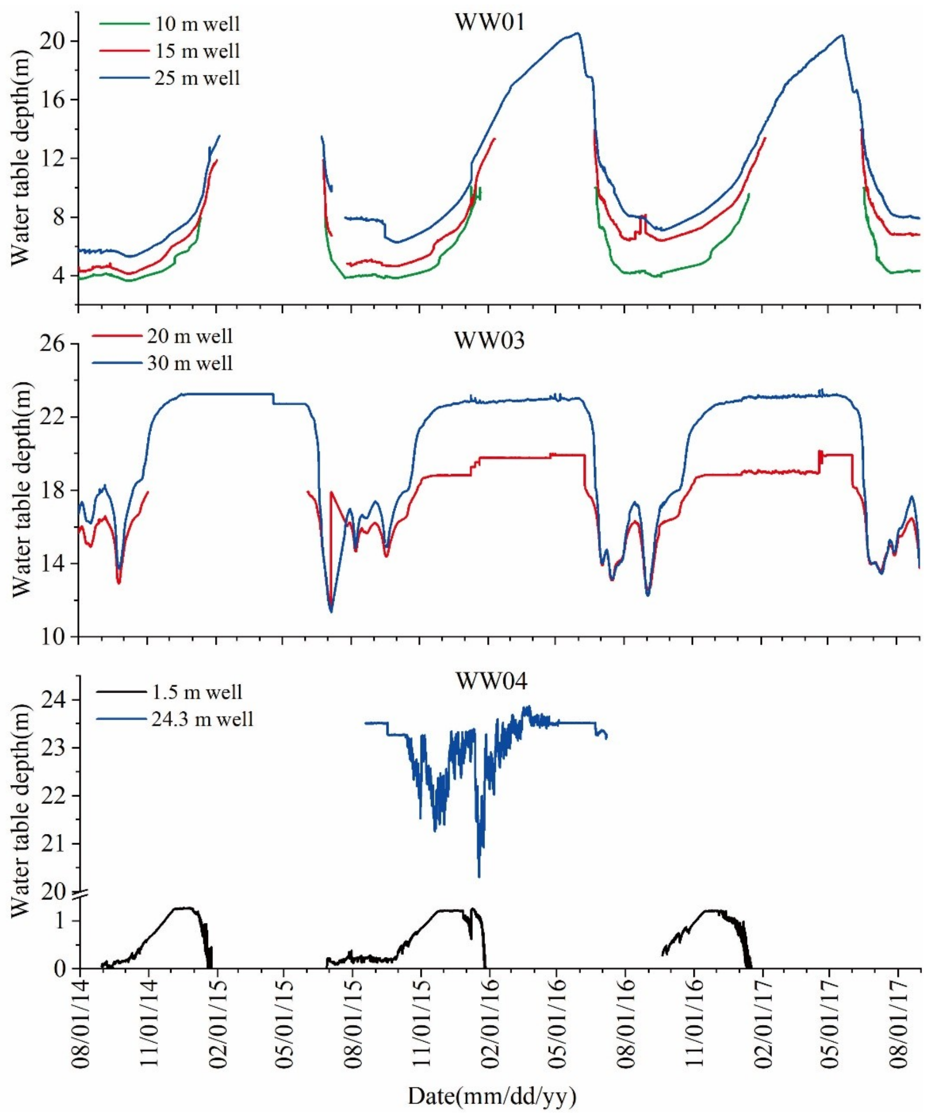

Fig. 3. Time series of water table depth in the wells at cluster WW01, WW03 and WW04.

The groundwater tables are deeper than wells screen depths during the missing data period.

4.2. ^{2}H and ^{18}O isotopes

The $\delta^{2}H$ and $\delta^{18}O$ of precipitation varied between −119‰ and −279‰ and −15.7‰ and −37.6‰, respectively. The Local Meteoric Water Line (LMWL) is $\delta^{2}H = 8.5\delta^{18}O + 22.6$ (R^2=0.9886, n=120; Fig. 4) (Tong et al., 2016; Ma et al., 2017). The $\delta^{2}H$ and $\delta^{18}O$ of groundwater, surface water, and snow/glacier meltwater derived from over 200 samples collected during a two-year period can be clustered into four main groups (Fig. 4): (1) groundwater within the permafrost zone at different depths (nested well set WW04 and other samples, Fig. 4a), (2) groundwater within the seasonal frost zone extracted from four depth-specific wells of nested well sets WW01 and WW03 and springs (Fig. 4b), (3) glacier/snow meltwater at different elevations in the catchment (Fig. 4a), and (4) stream water collected along the channel of the west tributary (Fig. 4c) and the east tributary (Fig. 4d), and at the catchment outlet (Fig. 4e).

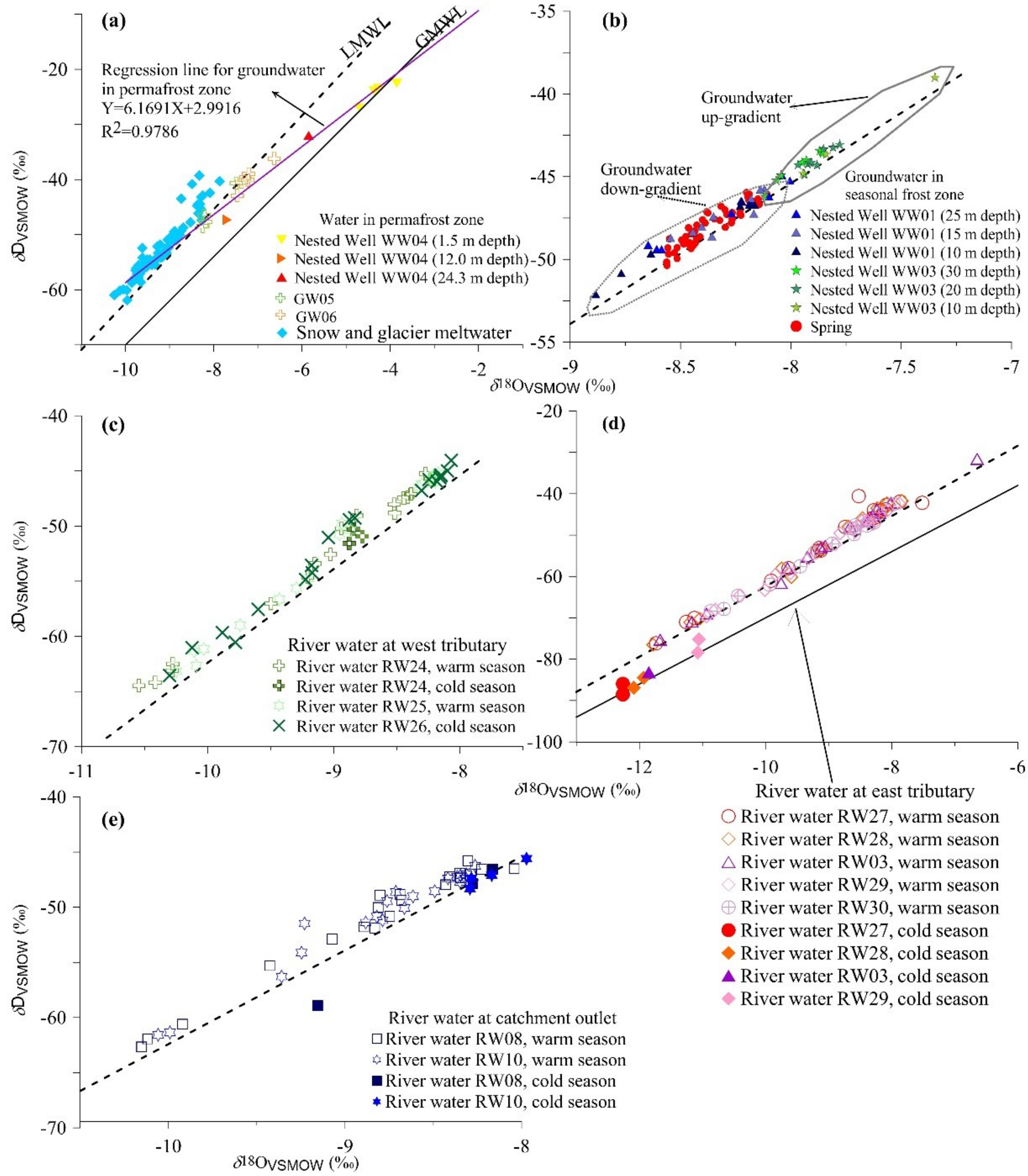

Fig. 4. The $\delta^{18}O$ and δD values measured in groundwater within the permafrost zone (a), groundwater in the seasonal frost zone (b), stream water from the west tributary (samples RW24, 25 and 26) (c), stream water from the east tributary (samples RW27, 28, 29, 03 and 30) (d), and main stream water at the catchment outlet (samples RW08 and 10) (e) for different seasons between September 2014 to January 2016.

The δ^2H and δ^{18}O of glacier/snow meltwaters were between −10‰ and −7.6‰, and −60‰ and −35‰, respectively (blue diamond symbol in Fig. 4a), which were larger than those in snowfall and glacial ice due to ablation (Li et al., 2015). The snow/glacier meltwater samples fall close to, but often slightly above, the LMWL in the δ^{18}O vs. δ^2H plot. Most of them exhibited isotopic values that overlap with the samples of groundwater from the seasonal frost zone and stream water. The regression line fitted to the groundwater samples from the permafrost zone crossed the LMWL line at the values of −50‰ for δ^2H and −8‰ for δ^{18}O, similar to the isotopic composition of glacier/snow meltwater.

The stream waters varied the most isotopically, with δ^{18}O values ranging between −12.3‰ and −6.7‰, and δ^2H values ranging between −88.5‰ and −31.6‰. Along a short reach of the west tributary, the δ^2H and δ^{18}O of the stream water varied in a relatively narrow range (Fig. 4c). However, the stream waters of the east tributary were relatively depleted in ^{2}H and ^{18}O during the cold season (solid symbols in Fig. 4d) and enriched in ^{2}H and ^{18}O during the warm season (hollow symbols in Fig. 4d). The stream water at the catchment outlet exhibited the opposite trend: the δ^{18}O and δ^2H values were more positive in the cold season (solid symbols in Fig. 4e) and negative in the warm season (hollow symbols in Fig. 4e).

The groundwater in the recharge zone of the seasonal frost area (nested wells set WW03) ranges between −8.1‰ and −7.7‰ for δ^{18}O and between −46‰ and −42‰ for δ^2H. Unexpectedly, the groundwater in the discharge zone (nested wells set WW01), with the δ^{18}O ranging between −8.9‰ and −8.0‰ and the δ^2H between −52‰ and −45‰, was more depleted and fluctuated in a wider range in heavy isotopes than that in the recharge zone. In general, the groundwater samples from wells at the recharge point (WW03) and discharge point (WW01) overlapped with the stream water samples collected along stream reaches during the warm season in the $\delta^{18}O$ vs. $\delta^{2}H$ plot (Fig. 4).

4.3 Water chemistry

The chemical compositions in west tributary stream waters were similar between warm and cold seasons; whereas, for stream waters from the east tributary, Ca^{2+}, Mg^{2+}, Si and Sr concentrations were higher and Cl^- concentration was lower in warm season than in cold season and other parameters exhibited similar values between the two seasons (Fig.5). Almost all major ions, minor elements (Si, Sr), total dissolved solids (TDS) and DIC were lower in the stream water samples from the two tributaries in comparison to the groundwater samples from springs and wells. However, the concentration of these solutes showed much higher variances for groundwater than for tributary water (Fig. 5). At the catchment outlet, the ion concentrations of stream water were approaching those measured in groundwater, and exhibited the largest geochemical variations in comparison to the other types of water on a seasonal basis. In January and April, the Ca^{2+}, Mg^{2+}, SO_4^{2-}, Si, Sr and TDS concentrations in shallow groundwater (from wells < 20 m in depth) were higher than those in deeper groundwater (from wells > 25 m in depth) (Fig. 5). The Na^+ and HCO_3^- concentrations, by contrast, were higher in the deep groundwater. From June to September, the Ca^{2+}, Mg^{2+}, K^+, Si, Sr, HCO_3^-, Cl^-, TDS and DIC concentrations in both the shallow and deep groundwaters were similar. However, the Na^+ concentration was still higher in the deep groundwater.

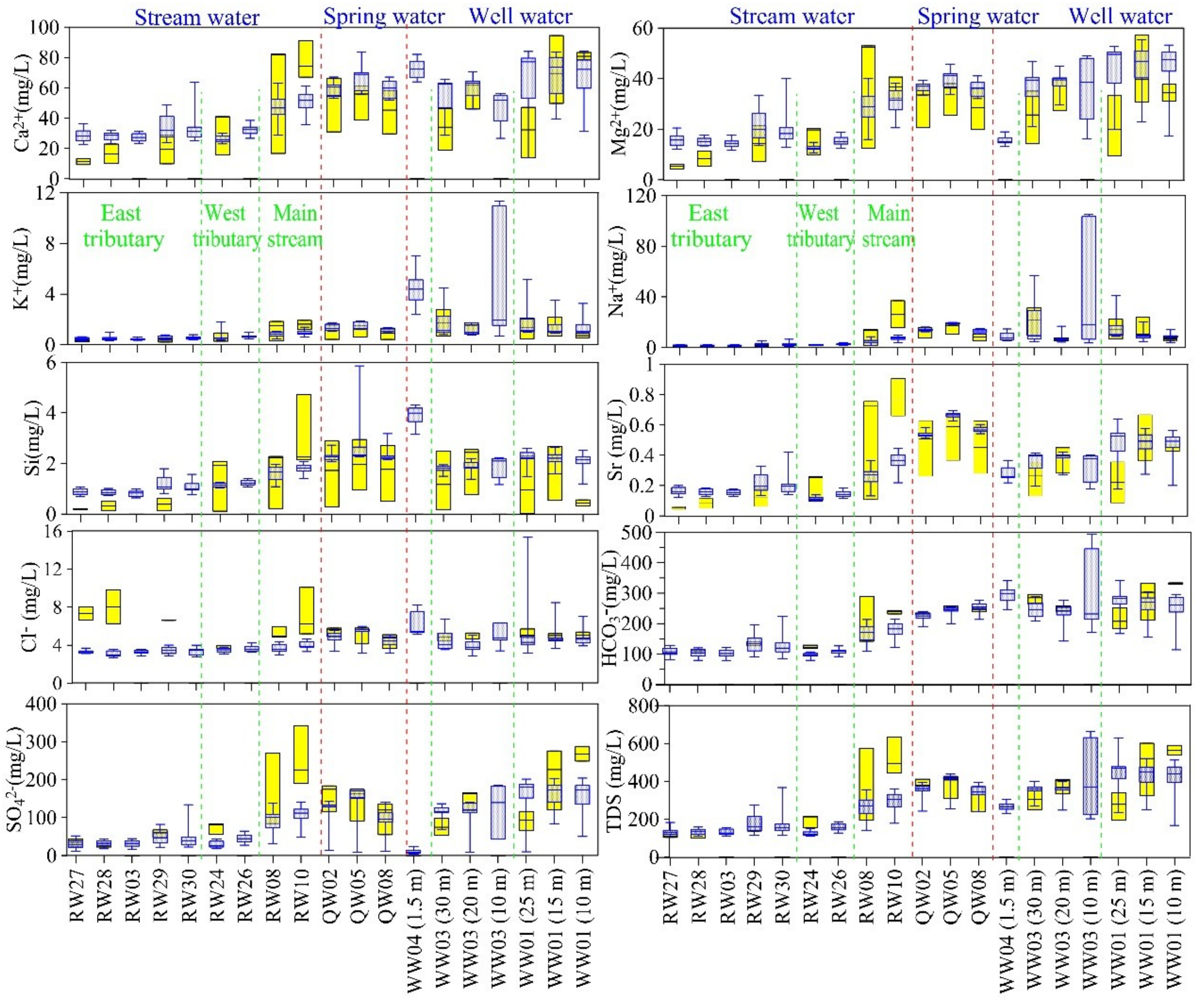

Blue bars present values in warm season; Yellow bars present values in cold season

Fig. 5. Box plots of major ions, Sr, Si and TDS concentrations measured within groundwater, river water, and springs from January to May (yellow color bar), and June to September (blue color bar), 2014-2016. Box range indicates lower quartile, mean (middle line) and upper quartile; whisker plots indicate maximum and minimum, respectively. Nested well set WW01 was located in the discharge zone of seasonal frost zone, WW03 in the recharge area of seasonal frost zone, and WW04 in the permafrost zone. The absence of yellow bars indicates that no samples were collected during the cold season.

The DOC concentration of stream water samples from the east tributary and catchment outlet was higher in the cold season than in the warm season, whereas the samples from the west tributary exhibited similar values during both seasons (Fig. 6). The DOC concentration in the suprapermafrost groundwater (from well WW04) within the permafrost zone was much higher than those in the groundwaters within the seasonal frost zone. The groundwater from well WW03 exhibited higher DOC concentration in cold season than in warm season, while that from WW01 had similar DOC values during both seasons (Fig. 6).

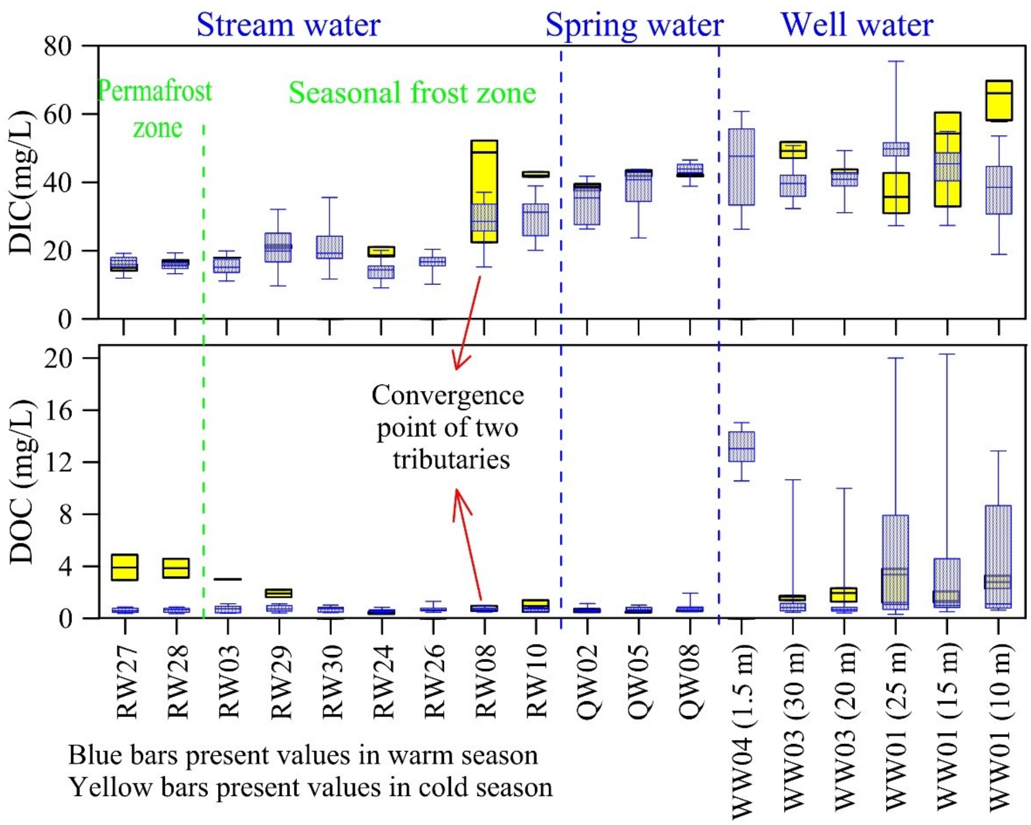

Fig. 6. Spatial changes in DIC and DOC in different types of waters. Samples are oriented from upstream to downstream, and were collected between January and April or May (yellow color bar) and June to September (blue color bar). Box range indicates lower quartile, mean (middle line) and upper quartile; whisker plots indicate maximum and minimum, respectively. The absence of yellow bars indicates that no samples were collected during cold

season.

The suprapermafrost groundwater and stream water within the permafrost zone exhibited higher major ions, Si, Sr, DIC and DOC concentrations in cold season than in warm season, which was especially true for DOC concentration (Fig. 7). These solutes remained relatively high concentrations in June, but deceased to their lowest values in July to August, and then increased again in late September. The opposite trends were observed for the DIC and DOC concentrations (Fig. 7). The geochemistry of groundwater and stream water in the seasonal frost zone exhibited the trend similar to that in the permafrost zone, except that the groundwater samples from the wells were relatively stable in geochemistry throughout the warm season (Fig. 8). The DOC concentration of groundwater in the seasonal frost zone showed no obvious increase in September. In comparison, the major ions, Si, Sr, DIC and DIC concentrations in stream water at the catchment outlet were quite dynamic with the general trends similar to those in the permafrost and seasonal frost zones (Fig. 9).

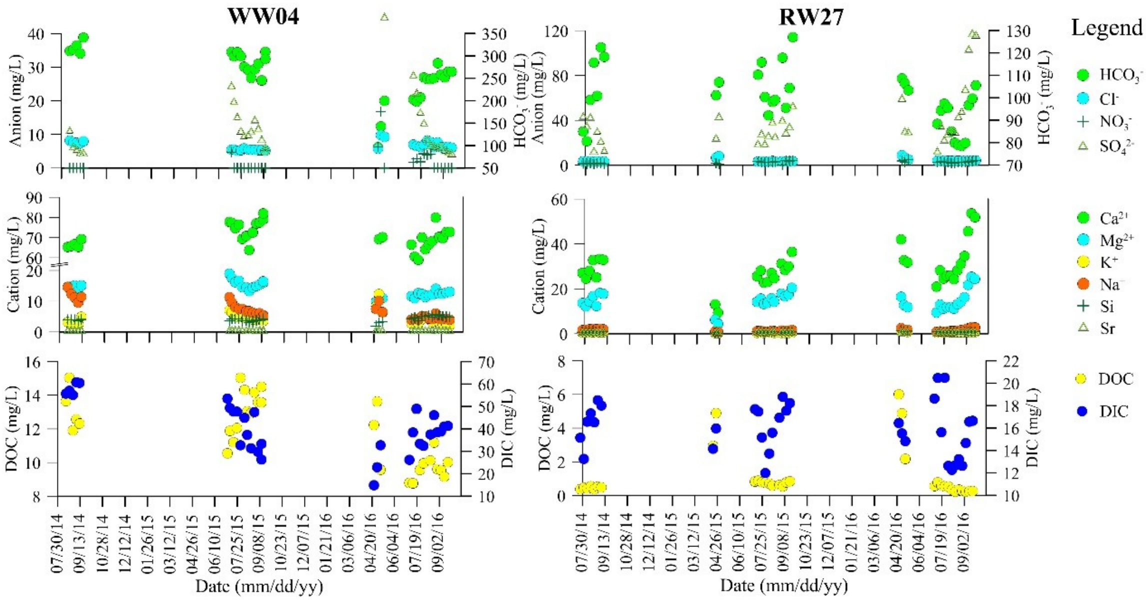

Fig. 7. Change in major ions, Sr, Si, DIC and DOC concentrations in suprapermafrost groundwater (WW04) and stream waters (RW27) from July 2014 to September 2016 within the permafrost area.

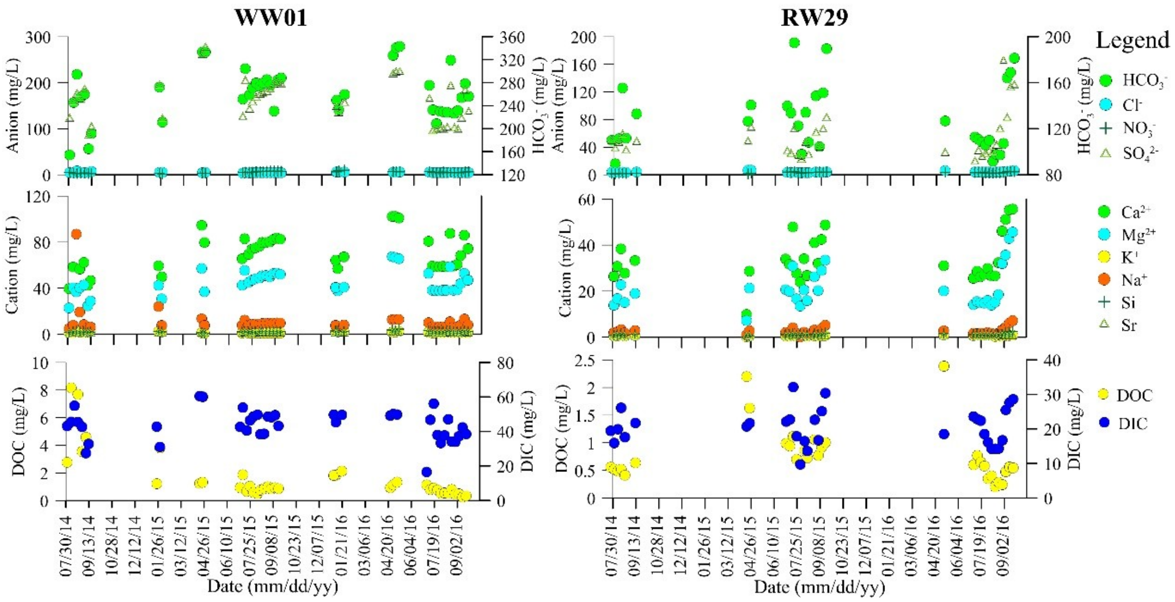

Fig. 8. Change in major ions, Sr, Si, DIC and DOC concentrations in groundwater (WW01) and stream waters (RW29) from July 2014 to September 2016 within the seasonal frost area.

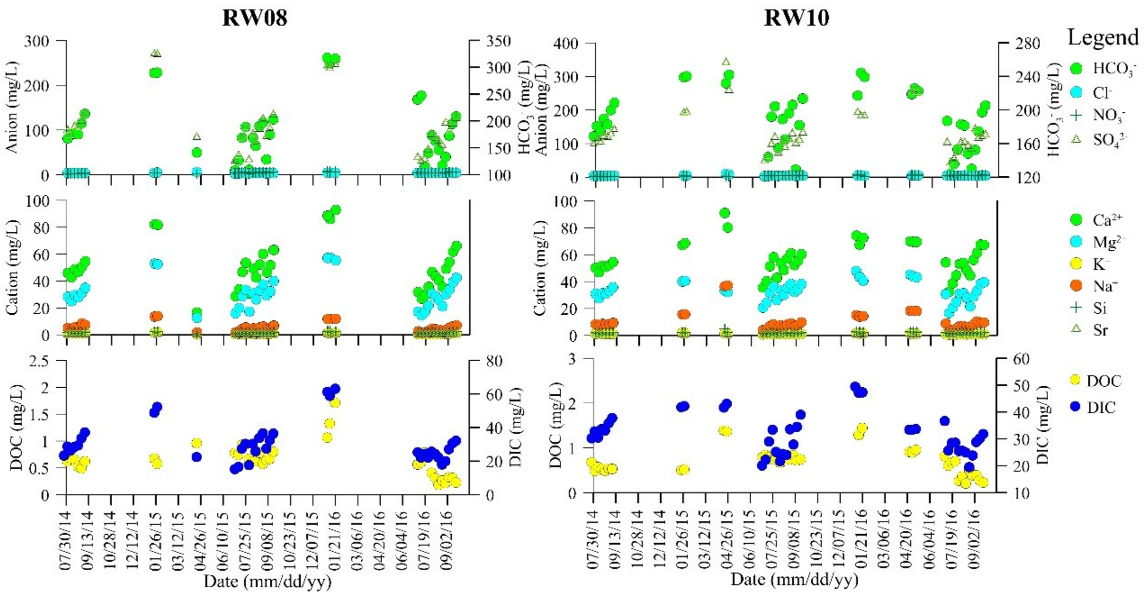

Fig. 9. Change in major ions, Sr, Si, DIC and DOC concentrations in main stream waters

from July 2014 to September 2016 at the catchment outlet.

4.4 The contributions of the waters from different flow paths to mainstream and associated uncertainties

4.4.1 The fractional contribution of different flow paths to mainstream

Though the precipitation and glacier/snow meltwater were the ultimate sources of the catchment discharge, they may be modified in isotopic signals during flow processes before entering the stream channel. Thus, it was difficult to evaluate the contribution of these 'ultimate sources' to the mainstream due to the overlap in their isotopic compositions. The water sources that directly recharged the axial channel of the Heihe River included stream-water from the east and west tributaries, shallow groundwater and deep groundwater. The contribution of groundwater to the mainstream is of concern in this study. Thus, the shallow groundwater, deep groundwater, and stream water from the two tributaries were treated as the dominant water sources and as geochemical endmembers. Their contributions to the mainstream were determined using the Bayesian model. The geochemistry of the tributary endmember was based on samples from RW27, RW28, RW29, RW30, RW24, RW25 and RW26 from both the permafrost and seasonal frost zones since the change in δ^{18}O and δD for different stream waters at the same sampling time falls within a narrow range (Fig. 4). The O and D isotope values of shallow groundwaters, which follow a shallower flow path and contact with permafrost or seasonal frost, were similar to each other within the same season (Fig. 8). Thus, the D and O values of isotope values in the nested wells at sites WW01 were used to represent shallow groundwaters. Deep groundwater follows a deep flow path through the aquifer to the mainstream (Evans et al., 2015). Given that groundwater samples were not obtained from wells at depths >30 m, the isotopic compositions of spring water at a lower elevation which was considered as discharge of deeper groundwater (Ma et al., 2017) was selected as an endmember for deep groundwater. Tributary stream-waters, shallow groundwater, and deep groundwater exhibited distinctly different values for δ^{18}O and D in comparison with the stream waters at catchment outlet at different seasons (Fig. 5).

The results of the Bayesian mixing model show that the contribution of tributary streams to the mainstream discharge varied most (Fig. 10). It only accounted for ~ 5% of total mainstream discharge in January, ~ 5%−20% in April and May, ~ 20%−60% in June to August, and ~ 10%−30% in late September. Though differing between different seasons, the contribution of subsurface flow from aquifers always dominated the catchment discharge. Groundwater contributed ~ 95% of total mainstream discharge in January, decreased to ~ 80%−95% in April to May, and further decreased to ~ 40%−80% from June to August, then increased to ~ 70%−90% in late September. The contribution of groundwater following the deep flow path remained relatively constant across the two seasons (except for July in 2015), accounting for ~ 40% of the total mainstream discharge. In comparison, the contribution of groundwater from the shallow flow path varied significantly with the season, generally being higher in the cold season and lower in the warm season.

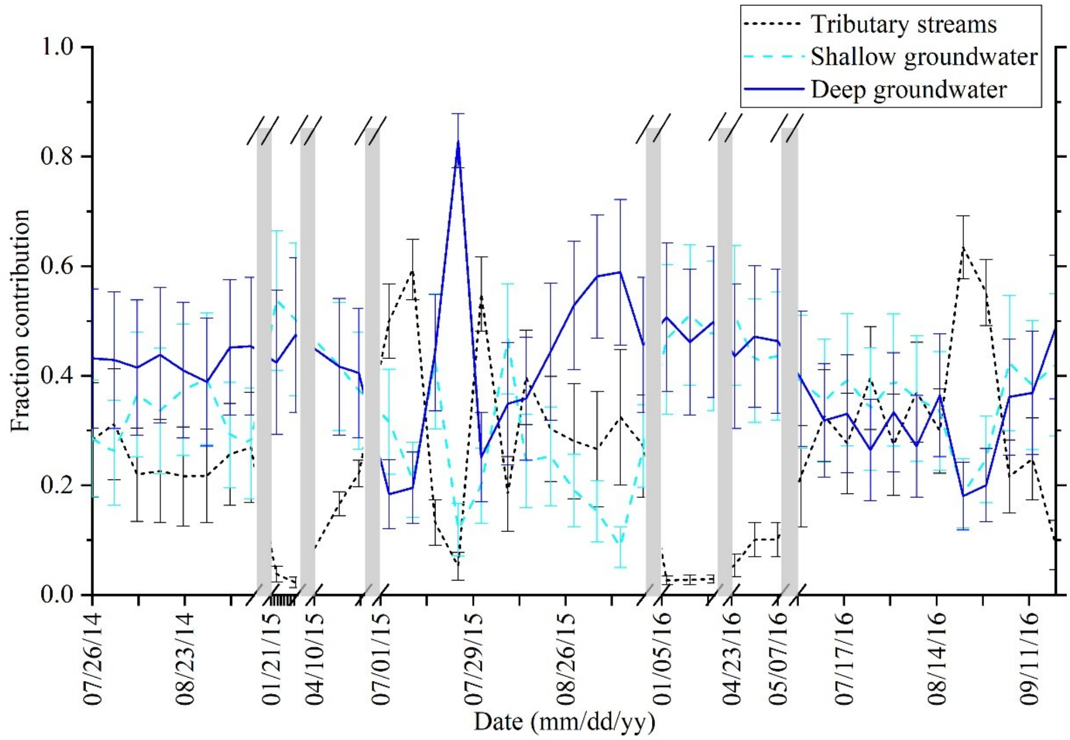

Fig 10. Time series graph of proportional contribution of three potential water sources to the main discharge channel of the Hulugou mainstream from July 2014 to September 2016 estimated by the BMC model. y axis error bars are the uncertainties produced in the BMC model.

4.4.2 Uncertainty in estimates of water flow path contributions

The uncertainty in the calculated fractional contribution was presented in Fig. 10. It may originate from isotope variability of the waters associated with each source and the statistical distribution of isotopic tracers. While the isotopic values differed between water sources, flows along the stream channel or through the groundwater system or at different seasons may increase the isotopic variability of the waters associated with each source.

The uncertainties in contribution percentage of the tributary stream in the cold season (1% to 5%) were much smaller than those in the warm season (10% to 20%). The major reason should be that isotopic values along tributary stream channel in the warm season have larger variation than the cold season. In comparison, the contributions of shallow and deep groundwater exhibited higher uncertainties in the cold season (~25%), and lower uncertainties (15-20%) in the warm season. The larger uncertainties of the fraction of shallow and deep groundwater maybe because their $\delta^{18}O$ and δD values are relatively closer to each other compared to their differences with stream water composition.

5. Discussion

5.1 The control of permafrost and seasonal frost on groundwater and stream water interaction

5.1.1. Winter

The Bayesian model calculation confirmed that the groundwater contributed approximately 95% of mainstream discharge during the frozen period, indicating the release of groundwater stored under the frozen layer into stream since the water source and suprapermafrost aquifer were completely frozen. This addresses the significant impact of permafrost and seasonal frost on groundwater and stream water interaction during the frozen period.

Within the permafrost zone, both subpermafrost groundwater and stream water received a negligible recharge due to the frozen water source, resulting in the dry of the east tributary and the upper part of the west tributary. In the west tributary subcatchment, the groundwater stored in pro-glacial moraine and talus deposits discharged as a spring via talik (QW01 in Fig. 1). This perennial spring as observed during our field investigation fed the lower part of west tributary within the permafrost zone. The narrow range of the geochemical concentrations, $\delta^{18}O$ and δD values among stream waters along the west tributary reach and between the seasons also confirmed the constant water source for stream water, i.e. spring QW01 (Fig. 4, 5 and 7). The subpermafrost groundwater may discharge to the aquifers in the seasonal frost zone, but the lateral outflow should be very limited since the porous deposit connecting the permafrost and seasonal frost aquifers was very thin which was possibly frozen (Ma et al., 2017).

The west tributary was dry after entering the seasonal frost zone, indicating that all stream flux infiltrated into the aquifer via the local melt zone; while no streamflow recharge occurred in the east tributary since the stream was dry. Comparing with the thawing/thawed period, the hydraulic gradient between the top and base of the piedmont sloping plain within the seasonal frost zone is relatively small (Fig. 3), indicating a very limited recharge relative to discharge and a very slow flow rate. Ca^{2+}, Mg^{2+}, Sr, HCO_3^-, SO_4^{2-} concentrations in deeper groundwaters (from depth >15 m aquifer) were smaller than those in shallower depth in the frozen season (Fig. 5). It seems contradictory to the longer residence time resulted from the slow rate of groundwater. However, weathering of less soluble minerals, such as quartz and K-feldspar, may be an important contributor of solutes in deeper soil profiles; while the dissolution of carbonate minerals such as calcite and dolomite as well as the weathering of the silicates are likely responsible for the chemical composition of the groundwater in the shallower parts of the aquifer (Hu et al., 2019). The stream channel remained dry within the seasonal frost zone until down to the catchment outlet, where the springs such as QW10 emerged at the base of the piedmont sloping plain and fed the stream water. The emergence of the springs indicates the release of groundwater stored in the aquifer within the seasonal frost zone since the surface water sources were frozen and the lateral flow from the permafrost zone was very limited. This was evidenced by the similar TDS, major ions concentrations and ^{18}O and ^{2}H compositions between groundwater at discharge zone (as shown in WW01), springs and mainstream water (RW08 and 10) (Fig. 8 and 9). The above analysis illuminates the mechanism of how the groundwater contributed a high percentage of total mainstream discharge and maintained the streamflow over the frozen period.

5.1.2. Spring

The thawing of the frozen deposits led to two different ways of exchange between groundwater and stream water within the permafrost zone. Firstly, spring (QW09) in east tributary subcatchment recovered and the discharge of spring (QW01) in west tributary subcatchment increased as observed during field investigation due to the thawing of the moraine sediments and the recharge of melting glacier-snow. The springs fed the tributary stream waters and further increased the streamflow which was already recharged by melting glacier-snow at a higher elevation (Chang et al., 2018; Hu et al., 2019). This was confirmed by the overlap of most glacier/snow meltwater samples with groundwater and stream water samples in the $\delta^{18}O$ vs δD plot (Fig.4). The second interaction way is via the shallow thawed soil. The active layer began to thaw but the thawing depth was small (Ma et al., 2017), leading to a small storage capacity of suprapermafrost reservoir as indicated by a near-surface water table (Fig. 3). The underlying frozen layer inhibited groundwater from infiltrating into deep mineral soil horizons, constraining it within shallow organic soil horizons. Thus, the ice meltwater from suprapermafrost aquifer and infiltrated glacier/snow meltwater flowed through the shallow organic soil and discharged to stream at the favorable location, which was evidenced by a higher DOC and lower DIC concentrations in both streams and suprapermafrost groundwater (Fig. 6 and 7). A thin layer of salt on the soil surface in the permafrost zone was observed in the frozen period during our field investigation, which may be caused by the mineral precipitation during the soil freeze process (Wang et al., 2018). The water, that flowed through this shallow soil layer, had higher Cl^- and Na^+ concentrations and depleted ^2H and ^{18}O compositions as indicated in water samples of RW27 and WW04 (Fig.4 and 7), which further confirmed the discharge of shallow groundwater into stream water. Followed by the above processes, the chemistry of stream water had a significant fingerprint of suprapermafrost groundwater.

After flowing into seasonal frost zone, the dry of the east tributary and the decreased streamflow of the west tributary stream were observed at the top of the piedmont sloping plain during field investigation (Fig. 2), suggesting that the stream water infiltrated into groundwater via localized taliks. This was also confirmed by the rapid rise of groundwater level at the top of the piedmont sloping plain since no precipitation infiltration could occur due to the frozen of the lower part of seasonal frost (Fig. 3). DOC concentration in groundwater from the seasonal frost zone was expected to decline and solute concentrations increase in response to deeper flow pathways and enhanced soil-water contact time (Frey and McClelland 2009; Petrone et al. 2006). However, our results show that the major ions and DOC concentrations in both the groundwater and stream water increased (Fig. 9), further indicating the effect of tributary stream water with the chemical fingerprint from permafrost zone on groundwater within the seasonal frost zone via infiltration. The west tributary streamflow flowed continuously until it merged into mainstream even after infiltrating into groundwater at the top of the piedmont sloping plain due to the increased streamflow from permafrost zone as previously analyzed. This explains the increased contribution fraction of tributary streams to mainstream with 10 to 20%. The groundwater at the base of the piedmont sloping plain discharged as springs (QW08, QW02-05) or directly discharged to the mainstream as base flow (Ma et al., 2017), and groundwater contribution fraction decreased to 80-90% compared to frozen period due to the inflow from tributaries into mainstream.

5.1.3. Summer

The continued thawing of moraine and talus deposits as well as fluvioglacial deposits within the permafrost zone, led to the increase in the spring discharge and change of the groundwater flow paths, further affecting the stream and groundwater interaction. The springs in the west tributary subcatchment exhibited the largest discharge among the year since the recharge source (glacier-snow meltwater) reached its largest volume and the thawed moraine aquifers with high hydraulic conductivity can rapidly transfer water from recharge to discharge points. Correspondingly, the west tributary streamflow increased due to the enhanced recharge from glacier-snow meltwater and springs. This was also suggested by the decreased DOC, DIC and major ions concentrations in stream water due to the dilution (Fig. 6 and 7). The active layer in east tributary subcatchment reached the maximum thaw depth and thus the storage capacity of suprapermafrost reservoir increased. However, supported by extensive recharge from local precipitation and overland flow, the suprapermafrost groundwater table rose to near the land surface and even exfiltrated to support surface water (Fig. 3). The very good recharge condition and shallow flow paths were suggested by a decrease in DOC, DIC, major ions, Si and Sr concentrations in suprapermafrost groundwater (Fig.7). With the thinning out of the supra- and subpermafrost aquifers at the boundary between permafrost and seasonal frost zones, the supra- and subpermafrost groundwaters were mainly discharged directly into streams, or as seeps and springs at the upper portions of the hill slopes and then entered into streams or aquifers in the seasonal frost zone. Due to the enhanced recharge by glacier-snow meltwater, springs and surface runoff as well as rainfall, the streamflow greatly increased in the permafrost zone (Fig. 2).

The completely thawed seasonal frost favored the infiltration of the stream water into groundwater along the channel within the seasonal frost zone. The great rise of the water table at the top of the piedmont sloping plain indicated that a large volume of tributary stream waters infiltrated into porous aquifer when they entered the piedmont plain (Fig. 3). This was also suggested by the larger variability of concentrations of major ions, Si, Sr and TDS in shallow groundwater (10 m depth well) compared to that in deeper groundwater (Fig.5). Both the east and west tributary streamflows were still continuous in the downstream after infiltration due to the largely increased stream flux from the permafrost zone (Fig. 2). The difference in hydrogeochemistry between shallower parts (<20 m depth) and deeper parts (20–30 m) of the aquifer among different seasons suggested that different flow paths existed in the aquifers throughout the year (Hu et al., 2019) (Fig. 5). However, the most ions and TDS concentrations in the groundwater from different depths became closer during the thawed period, indicating that the waters from different flow paths were more interconnected. The increased groundwater hydraulic gradient enhanced the groundwater discharge to the mainstream, and the increased groundwater level enlarged the recharge length of stream channel (Fig.3).

At the catchment outlet, the contribution of tributary streams to the mainstream reached the largest value (20%-60%) as shown by Bayesian model results (Fig. 10), which was also indicated by the general decreased trend of major ions, Sr, Sr, DOC and DIC concentrations in mainstream due to the surface water dilution. The variations in contribution fraction from tributary streams led to a different mix ratio between groundwater and stream, resulting in a dynamic change in major ions, Sr, Sr, DOC and DIC concentrations in mainstream waters (Fig. 9). The similar stream and groundwater exchange pattern from bedrock mountain to the catchment outlet in the thawed period was also reported in Sierra Nevada of CA (Ciruzzi & Lowry, 2017), Peru (Somers et al., 2016), and Swiss Alps (Volze, 2015).

5.1.4 Autumn

The release of groundwater stored in aquifer into stream dominated the groundwater and stream water interaction again as indicated by the increased groundwater contribution fraction to mainstream flow (Fig. 10). This should be caused by the freezing of the sediments from the top down and the part of water sources.

The discharge of springs from moraine within the permafrost zone greatly deceased compared to the thawed period due to the less recharge caused by partly frozen glacier-meltwater and sediments. The decreased spring discharge and precipitation resulted in the large decline of tributary streamflow (Fig. 2). The suprapermafrost aquifer on the planation surfaces became confined and the part of groundwater within it converted to ice due to the frozen of the upper part of the aquifer. Thus, the aquifer storage decreased, releasing the groundwater into the surface water via localized talik. This process was evidenced by the increased DOC, DIC, major ions concentrations as well as depleted D and O compositions due to the fractionation between ice and water in both suprapermafrost and stream water samples as shown in Fig.4 and 7 (Belzile et al., 2002; Guo et al., 2012).

The tributary streamflows significantly declined after entering the piedmont sloping plain within the seasonal frost zone (Fig. 2), indicating that most flux from tributaries infiltrated into the porous aquifer via talik under streambed. However, the infiltration of stream flux during freeze-back period was much less than the thawed period, as suggested by a decline in groundwater table and an increase in major ions, Si and Sr concentrations at the top of the piedmont sloping plain (Fig. 3 and 8). The discharge of groundwater to mainstream via springs or baseflow at catchment outlet was also greatly decreased, as confirmed by the increased major ions and DIC concentrations in mainstream waters as well as lowered groundwater hydraulic gradient (Fig.3 and 9). However, the fraction of groundwater contribution increased since the tributary streamflow contribution decreased (Fig. 10).

5.2 The function of groundwater in maintaining streamflow at the catchment outlet

Recent studies have shown that groundwater storage and release may be more important in maintaining streamflow in the alpine environment than previously thought (e.g., Chang et al., 2018; Kobierska et al., 2015; McClymont et al., 2010). For example, studies in an alpine catchment in Colorado Front Range indicated that groundwater flowing from talus can account for 75% of streamflow during storms and the winter baseflow period (Clow et al., 2003). Field studies in other alpine catchments also showed that even during the high-flow melt period groundwater can contribute more than half of the streamflow (e.g., Andermann et al., 2012; Hood et al., 2006; Liu et al., 2004; Shaw et al., 2014). As shown by the Bayesian mixing model (Fig. 10), our results also confirmed that groundwater contribution plays a dominant role in maintaining streamflow in the alpine catchment.

Among three types of aquifers in the Hulugou catchment, previous studies have argued that pro-glacial moraines and talus slopes, despite their large storage potential, transmitted water quickly and thus were unlikely to sustain baseflow in the alpine catchment (Clow & Sueker, 2000). The present study suggests that groundwater storage and transmission in the piedmont plain likely dominated subsurface flow in the Hulugou catchment. This was also evidenced by comparing the contributions of surface water from mountains (via the two tributaries) and groundwater from piedmont plain to the stream discharge (Fig. 10). The seasonal variation in water storing and releasing of the aquifer composed of fluvioglacial and moraine deposits in the piedmont plain was mainly driven by the seasonal changes of the groundwater hydraulic gradient between the recharge area and discharge area.

As discussed in the above section and our previous studies (Chang et al., 2018; Ge et al., 2018; Ma et al., 2017), groundwater was recharged at the top of the piedmont plain by the seepage of streams and the lateral inflow from high mountains and hills in the permafrost zone, and discharged as baseflow to the Hulugou stream at the base of the piedmont plain. The recharge processes occurred mainly during the thawing/thawed seasons, causing the water table in the recharge area to be much higher than that during the cold seasons and to fluctuate in response to heavy rainfall events (Ma et al., 2017). Since the water table dynamics in the discharge area confined to a narrow range throughout the year, the hydraulic gradient between the recharge area and the discharge area would remain high overall during the thawed seasons (Fig. 3). This would lead to a large seepage flux from the aquifers to the Hulugou stream at the base of the plain. In the early freezing period when the recharge decreased significantly, the hydraulic gradient would decrease rapidly with groundwater release to the Hulugou stream. The decreasing hydraulic gradient would, in turn, slow down the release of groundwater and the decline of hydraulic gradient, preventing the aquifers from being drained out during the cold seasons. With this feedback mechanism, the aquifers in the piedmont plain have the ability to switch in hydrological functions from the rapid transmission of groundwater (water conduction function) during the warm seasons to the slow release of stored groundwater (baseflow maintenance function) during the cold seasons.

The shallow and deep groundwater contributed 80-95% of the total flow to the mainstream, being a key factor in maintaining streamflow in the cold season. The deeper groundwater flow analyzed here is stored in a regional flow system (Evans et al., 2015), which has a large temporal capacity to adjust for water storage between seasons and from one year to the next. The contribution of deep groundwater flow to the mainstream varied small between different seasons, and therefore flow regimes. However, shallow groundwater flow flux in the piedmont plain was significantly affected by the permafrost and seasonal frost distribution and freeze-thaw process, such as the frozen water source and sediments in the frozen period, and enhanced recharge in thawed period. Thus groundwater flow contribution to mainstream water varied between seasons.

Due to difficulties in hydrogeological investigation, field-based research in the headwater region of Heihe River has been focused on the surface components of the hydrological cycle, such as rainfall-runoff or snow accumulation and melt (Wang et al., 2018; Gao et al., 2018). This unintentionally caused to some extent an underestimate of the importance of groundwater in maintaining streamflow. Our study demonstrates that the aquifers within piedmont plain play key roles in regulating the rate and timing of the stream discharge from the Hulugou catchment, and this kind of "mountain-piedmont plain" catchment is common in the headwater region of Heihe River. The piedmont plains with thick unconsolidated deposits are widely distributed along the mainstream and its large tributaries, so that the glacier-snow meltwater and rainfall runoff from mountains must flow through these plains and probably percolate down into the coarse-textured aquifers largely before traveling to the rivers (Ma et al., 2017). The groundwater storage and flow within these piedmont plains played a significant role in hydrological regulation in the headwater region of Heihe River. More field-based hydrogeological research and modeling work should be conducted to better understand what groundwater contributes to river runoff and how groundwater may buffer the effects of climate change on mountain rivers.

6. Conclusions

The surface water and groundwater interaction in the middle and low latitude alpine catchments in the Qinghai-Tibet plateau may differ from those in arctic and subarctic areas due to the co-distribution of discontinuous permafrost and seasonal frost, and occurrence of concentrated precipitation and glacial/snow meltwater in the warm season. The contribution of groundwater to the Heihe River was previously unquantified in the headwater regions of the Heihe River located along the eastern Qinghai-Tibet Plateau, China. This study employed hydraulic data, chemical and isotopic analyses to assess spatial and temporal changes in groundwater and surface water interactions controlled by the distribution of permafrost and seasonal frost and soil freeze-thaw process.

The exchange relationships between groundwater and surface water were complex along the different landforms of the catchment. The freeze-thaw process of pro-glacial moraine and talus deposits in the permafrost zone controlled the discharge rate of springs into tributary streams. Further, the active layer freeze-thaw processes altered the storage capacity of suprapermafrost aquifer and thus exchange relationships between suprapermafrost groundwater and surface water in different seasons. The groundwater and surface water interaction in the seasonal frost zone differed from that in the permafrost zone. The freeze-thaw cycle of the seasonal frost controlled the infiltration of stream flux at the top of the piedmont plain and along the channel, thus affecting the groundwater hydraulic gradient. The seasonal frost at the base of the piedmont plain confined the groundwater level and further affected the flow from the aquifer to the mainstream during the frozen period. Correspondingly, the Bayesian model results revealed significant seasonal variability in the contribution of tributary streams and groundwater following the shallow flow path to the mainstream. In response to groundwater and stream water interaction controlled by the freeze-thaw process, the contribution from groundwater accounted for ~95% of the total mainstream discharge during the frozen period when soils were completely frozen, decreased to 80-95% during the thawing period when the soils started to thaw, further changed to 40-80% during the thawed period when the soils were completed thawed, and increased to ~70-90% during the freeze-back period when the soils started to freeze.

The results here highlighted the important role of groundwater in maintaining the Heihe river discharge at different seasons and between years, especially during the cold season when the soils and water sources were frozen and few surface water generated. Thus, it implied that water resource estimation and management should consider the effects of permafrost and seasonal frost on the contribution of groundwater to large rivers which has been neglected for a long term.

Acknowledgements

This research was financially supported by National Natural Science Foundations of China (NSFC- 91325101 and 41521001), the Strategic Priority Research Program of Chinese Academy of Sciences (No. XDA20100103). The data in this study will be provided through Zenodo website by acceptance of this manuscript.

References:

Anderson, L., Birks, J., Rover, J., & Guldager, N. (2013). Controls on recent Alaskan lake changes identified from water isotopes and remote sensing. Geophysical Research Letter, 40, 3413–3418. doi:10.1002/grl.50672.

Andermann, C., Longuevergne, L., Bonnet, S., Crave, A., Davy, P., & Gloaguen, R. (2012). Impact of transient groundwater storage on the discharge of Himalayan rivers. Nature Geoscience, 5(2), 127-132.

Arendt, C. A., Aciego, S. M., & Hetland, E. A. (2015). An open source Bayesian Monte Carlo isotope mixing model with applications in Earth surface processes. Geochemistry, Geophysics, Geosystems, 16, 1274–1292.

Belzile C., Gibson, J.A.E., & Vincent, W.F. (2002). Colored dissolved organic matter and dissolved organic carbon exclusion from lake ice: implications for irradiance transmission and carbon cycling. Limnology Oceanography, 45(5): 1283–1293. DOI: 10.4319/lo.2002.47.5.1283

Brassard, P., Waddington, J. M., Hill. A. R., & Roulet, N. T. (2000). Modelling groundwater±surface water mixing in a headwater wetland: implications for hydrograph separation. Hydrological Processes, 14, 2697-2710.

Cable, J., Ogle, K., & Williams, D. (2011). Contribution of glacier meltwater to streamflow in the Wind River Range, Wyoming, inferred via a Bayesian mixing model applied to isotopic measurements. Hydrological Processes, 25, 2228–2236.

Chang, Q., Ma, R., Sun, Z., Zhou, A., Hu, Y., & Liu, Y. (2018). Using isotopic and geochemical tracers to determine the contribution of glacier-snow meltwater to streamflow in a partly glacierized alpine-gorge catchment in northeastern Qinghai-Tibet Plateau. Journal of Geophysical Research-Atmospheres, 123, 10037-10056.

Chen, R., Han, C., Song, Y., & Liu, J. (2014a). Data are obtained from 4 levels on 10m meteorological tower in Hulugou sub-basin of alpine Heihe River. Heihe Plan Science Data Center. https://doi.org/10.3972/heihe.078.2014.db.

Chen, R. S., Song, Y. X., Kang, E. S., Han, C. T., Liu, J. F., Yang, Y., Qing, W., & Liu, Z. (2014b). A cryosphere-hydrology observation system in a small alpine watershed in the Qilian Mountains of China and its meteorological gradient. Arctic, Antarctic, and Alpine Research, 46(2), 505-523.

Clow, D. W., Schrott, L., Webb, R., Campbell, D. H., Torizzo, A., & Dornblaser, M. (2003). Ground water occurrence and contributions to streamflow in an alpine catchment, Colorado Front Range. Ground Water, 41(7), 937-950.

Clow, D. W., & Sueker, J. K. (2000). Relations between basin characteristics and stream water chemistry in alpine/subalpine basins in Rocky Mountain National Park, Colorado.

Water Resources Research, 36(1), 49-61.

Ciruzzi, D., & Lowry, C. (2017). Impact of complex aquifer geometry on groundwater storage in high−elevation meadows of the Sierra Nevada Mountains, CA. Hydrological Processes, 31(10): 1863-1875.

Cheng, G., & Jin, H. (2013). Permafrost and groundwater on the Qinghai-Tibet Plateau and in northeast China. Hydrogeology Journal, 21(1), 5–23.

Davis, P., Syme, J., Heikoop, J., Fessenden-Rahn, J., Perkins, G., Newman, B., Chrystal, A. E., & Hagerty S. B. (2015). Quantifying uncertainty in stable isotope mixing models, Journal of Geophysical Research: Biogeosciences, 120, 903–923. doi:10.1002/2014JG002839.

Dornblaser, M.M., & Striegl, R.G. (2007). Nutrient (N, P) loads and yields at multiple scales and subbasin types in the Yukon river basin. Alaska. Journal of Geophysical Research, 112. G04S57. doi:10.1029/2006JG000366.

Dornblaser, M.M., & Striegl, R.G. (2009). Suspended sediment and carbonate transport in the Yukon river basin, Alaska: fluxes and potential future responses to climate change. Water Resources Research, 45, W06411. doi:10.1029/2008WR007546.

Evans, S. G., Ge, S. M., & Liang, S. H. (2015). Analysis of groundwater flow in mountainous, headwater catchments with permafrost. Water Resources Research, 51, 9564–9576.

Frey, K. E., & McClelland, J. W. (2009). Impacts of permafrost degradation on arctic river biogeochemistry. Hydrological Processes, 23, 169–182, doi:10.1002/hyp.7196.

Frey, K.E., Siegel, K.E., & Smith, L.C. (2007). Geochemistry of west Siberian streams and their potential response to permafrost degradation. Water Resources Research, 43, W03406. doi:10.1029/2006WR004902.

Gao, B., Yang, D., Qin, Y., Wang, Y., Li, H., Zhang, Y., & Zhang, T. (2018). Change in frozen soils and its effect on regional hydrology, upper Heihe basin, northeastern Qinghai-Tibetan Plateau. Cryosphere, 12, 657-673.

Garey, S. K., Boucher, J. L., & Duarte, C. M. (2013). Inferring groundwater contributions and pathways to streamflow during snowmelt over multiple years in a discontinuous permafrost subarctic environment (Yukon, Canada), Hydrogeology Journal, 21, 67–77.

Ge, M., Ma, R., Sun, Z., Long, X., Xing, W., Wang, S., & Yin, M. (2018). Using heat tracer to estimate river water and groundwater interactions in alpine and cold regions: A case study of Hulugou watershed in upper reach of Heihe River (in Chinese). Earth Science, 43(11), 4246-4255.

Guo, L.D., Cai, Y.H., Belzile, C., & Macdonald, R.W. (2012). Sources and export fluxes of inorganic and organic carbon and nutrient species from the seasonally ice-covered Yukon River. Biogeochemistry, 107(1-3), 187-206. DOI: 10.1007/s10533-010-9545-z

Hood, J. L., Roy, J. W., & Hayashi, M. (2006). Importance of groundwater in the water balance of an alpine headwater lake. Geophysical Research Letter, 33(13). L13405.

Hu, Y., Ma, R., Wang, Y., Chang, Q., Wang, S., Ge, M., Bu, J., & Sun, Z. (2019). Using hydrogeochemical data to trace groundwater flow paths in a cold alpine catchment, Hydrological Processes, 33(14): 1942-1960.

Jia, Y., Ding, X., Qin, C., & Wang, H. (2009). Distributed modeling of landsurface water and energy budgets in the inland Heihe River Basin of China, Hydrology and Earth System Sciences, 13, 1849-1866. doi:10.5194/hess-13-1849-2009.

Kobierska, F., Jonas, T., Kirchner, J. W., & Bernasconi, S. M. (2015). Linking baseflow separation and groundwater storage dynamics in an alpine basin (Dammagletscher, Switzerland). Hydrology and Earth System Sciences, 19(8), 3681-3693.

Li Z., Feng Q., Liu W., Wang T., Cheng A., Gao Y., Guo X., Pan Y., Li J., Guo R., & Jia

B. (2014). Study on the contribution of cryosphere to runoff in the cold alpine basin: A case study of Hulugou River Basin in the Qilian Mountains. Global and Planetary Change, 122, 345–361.

Li, Z., Feng, Q., Liu, W., Wang, T., Guo, X., Li, Z., Gao, Y., Pan, Y., Guo, R., Jia, B., Song, Y., & Han, C. (2015). The stable isotope evolution in Shiyi glacier system during the ablation period in the north of Tibetan Plateau, China. Quaternary International, 380-381, 262-271.

Liu, J., & Chen, R. (2016). Discriminating types of precipitation in Qilian Mountains, Tibetan Plateau. Journal of Hydrology: Regional Studies, 5, 20–32.

Liu, F. J., Williams, M. W., & Caine, N. (2004). Source waters and flow paths in an alpine catchment, Colorado Front Range, United States. Water Resources Research, 40, W09401. doi:10.1029/2004WR003076.

Lu, H., Wang, X., Ma, H., Tan, H., Vandenberghe, J., Miao, X., Li, Z., Sun, Y., An Z., & Cao, G. (2004). The plateau monsoon variations during the past 130 kyr revealed by loess deposit at northeast Qinghai-Tibet (China). Global and Planetary Change, 41(3-4), 207–214.

Ma, R., Sun, Z., Hu, Y., Chang, Q., Wang, S., Xing, W., & Ge, M. (2017). Hydrological connectivity from glaciers to rivers in the Qinghai-Tibet Plateau: roles of suprapermafrost and subpermafrost groundwater. Hydrology and Earth System Sciences, 21, 4803–4823.

McClymont, A. F., Hayashi, M., Bentley, L. R., Muir, D., & Ernst, E. (2010). Groundwater flow and storage within an alpine meadow-talus complex. Hydrology and Earth System Sciences, 14(6), 859-872.

Mondal, N.C., Singh V.P., Singh, V.S., & Saxena, V.K. (2010). Determining the interaction between groundwater and saline water through groundwater major ions chemistry. Journal of Hydrology. 388, 100–111.

O'Donnell, J.A., Aiken, G.R., Walvoord, M.A., & Butler, K. (2012). Dissolved organic matter composition of winter flow in the Yukon River basin: Implications of permafrost thaw and increased groundwater discharge. Global Biogeochemical Cycles, 26, GB0E06. doi:10.1029/2012GB004341.

Petrone, K.C., Jones, J.B., Hinzman, L.D., & Boone, R.D. (2006). Seasonal export of carbon, nitrogen, and major solutes from Alaskan catchments with discontinuous permafrost, Journal of Geophysical Research, 111, G02020. doi:10.1029/2005JG000055.

Rautio, A., & Korkka-Niemi, K. (2015). Chemical and isotopic tracers indicating groundwater/surface-water interaction within a boreal lake catchment in Finland. Hydrogeology Journal, 23:687-705.

Schuster, P.F., Striegl, R.G., Aiken, G.R., Krabbenhoft, D.P., Dewild, J.F., Butler, K., Kamark, B., & Dornblaser, M. (2011). Mercury export from the Yukon River Basin and potential response to a changing climate. Environmental Science and Technology, 45, 9262–9267. doi:10.1021/es202068b.

Shaw, G. D., Conklin, M. H., Nimz, G. J., & Liu, F. (2014). Groundwater and surface water flow to the Merced River, Yosemite Valley, California: ^{36}Cl and Cl−evidence. Water Resources Research, 50(3), 1943-1959.

Smith, L.C., Pavelsky, T.M., MacDonald, G.M., Shiklomanov, A.I., & Lammers, R.B. (2007). Rising minimum daily flows in northern Eurasian rivers: a growing influence of groundwater in the high latitude hydrologic cycle. Journal of Geophysical Research, 122, G04S47. doi:10.1029/2006JG000327.

Somers, L., Gordon, R., McKenzie, J., Lauta, L., Wigmore, O., Glose, A., Glas, R., Aubry-Wake, C., Mark, B., Baraer, M., & Condom, T. (2016). Quantifying groundwater-surface water interactions in a proglacial valley, Cordillera Blanca, Peru. Hydrological Processes, 30(17), 2915–2929.

Striegl, R.G., Aiken, G.R., Dornblaser, M.M., Raymond, P.A., & Wickland, K.P.

(2005). A decrease in discharge-normalized DOC export by the Yukon river during summer through autumn. Geophysical Research Letter, 32, L21413. doi:10.1029/2005GL024413.

Tong, J., Zhou, M., Sun, Z., Chang, Q., & Li, J. (2016). Water vapor sources of precipitation in the upper reaches of Heihe River: Evidence from stable water isotopes and air mass trajectory model (in Chinese), Journal of Arid Land Resource and Environment, 30, 151–156.

Utting, N., Lauriol, B., Mochnacz, N., Aeschbach-Hertig, W., & Clark, I. (2013). Noble gas and isotope geochemistry in western Canadian Arctic watersheds: tracing groundwater recharge in permafrost terrain. Hydrogeology Journal, 21, 79–91.

Volze, N. (2015). Characterization of Storage and Drainage Behavior of Alpine Slopes, Doctoral Thesis, University of Bayreuth, Switzerland.

Wang, Q., Zhang, T., Jin, H., Cao, B., Peng, X., Wang, K., Li, L., Guo, H., Liu, J., & Cao, L. (2017). Observational study on the active layer freeze–thaw cycle in the upper reaches of the Heihe River of the north-eastern Qinghai-Tibet Plateau. Quaternary International, 440 (Part B), 13–22.

Wang, Y., Yang, H., Gao, B., Wang, T., Qin, Y., & Yang, D. (2018). Frozen ground degradation may reduce future runoff in the headwaters of an inland river on the northeastern Tibetan Plateau. Journal of Hydrology, 564, 1153-1164.

Wei, W., Ma, R., Sun, Z., Zhou, A., Bu, J., Long, X., & Liu, Y. (2018). Effects of mining activities on the release of heavy metals (HMs) in a typical mountain headwater region, the Qinghai-Tibet Plateau in China. International Journal of Environmental Research and Public Health, 15(9), 1987. doi: 10.3390/ijerph15091987.

Woo, M. K. (2012). Permafrost hydrology. Berlin: Springer.

Woo, M., & Marsh, P. (2005). Snow, frozen soils and permafrost hydrology in Canada, 1999–2002. Hydrological Processes, 19, 215–229.

Table 1. Mean values, standard deviations (± SD) and number of samples used to determine chemical concentrations and H and O isotopic compositions in different types of waters from July to September, and from January to April or May. W refers to warm season; C refers to cold season; nh refers to sample numbers in warm season and nl refers to sample numbers in cold season. n.s. means that no samples were collected.

Chemical indicator (mg/L)		River waters		Spring	Well waters							Glacier meltwater	Snow meltwater
		periglacial and permafrost zone	seasonal frost zone		WW01 (25 m)	WW01 (<20m)	WW03 (30m)	WW03 (<20m)	WW04 (24.3m)	WW04 (1.5m)	WW04 (12m)		
		nh=48; nl=5	nh=129; nl=12	nh=99; nl=20	nh=19; nl=4	nh=50;nl=6	nh=19; nl=4	nh=25; nl=6	nh=1	nh=17	nl=1	nh=41	nh=20
Ca^{2+}	W	27.9±3.2	36.7±10.5	62.2±6.2	65.3±20.1	68.5±15.5	55.1±11.0	56.8±10.0	47.4	72.4±5.8	n.s.	19.8±11.4	9.4±10.6
	C	13.9±6.3	52.0±29.7	49.2±13.0	31.4±14.3	74.1±16.5	33.3±13.2	57.0±9.6	n.s.	n.s.	204.6	n.s.	n.s.
Na^{+}	W	1.5±0.4	3.5±2.2	16.2±2.5	24.5±42.5	10.5±11.3	17.6±15.1	7.8±4.0	23.3	8.6±2.8	n.s.	0.9±0.6	0.9±0.8
	C	1.1±0.4	12.0±13.0	12.7±5.0	14.5±7.8	10.9±6.9	21.1±10.6	6.7±1.3	n.s.	n.s.	221.0	n.s.	n.s.
Mg^{2+}	W	15.1±1.9	20.7±8.1	37.8±2.9	43.2±10.9	44.4±9.8	36.7±6.3	38±7.0	22.9	15.4±1.4	n.s.	7.7±4.3	1.8±1.5
	C	6.8±3.1	28.6±15.8	30.9±7.1	20.8±9.9	39.4±9.8	25.2±9.9	35.6±7.2	n.s.	n.s.	95.9	n.s.	n.s.
K^{+}	W	0.5±0.1	0.7±0.2	1.4±0.3	1.7±1.2	1.3±0.6	1.6±0.9	2±2.8	6.4	4.3±1.3	n.s.	1.7±0.9	1.7±1.9
	C	0.4±0.1	1.1±0.6	1.0±0.5	1.3±0.8	1.3±0.7	1.7±1.1	1.4±0.4	n.s.	n.s.	9.7	n.s.	n.s.
SO_4^{2-}	W	30.7±9.5	59.1±33.9	132±40.0	158.9±51.6	160.3±41.9	115±16.8	117.7±40.3	64.7	10.2±5.5	n.s.	22.6±23.8	5.1±2.3
	C	31.6±10.3	161.9±103.9	145.2±34.4	92.4±22.0	230.8±63.0	74.9±24.6	148.8±26.5	n.s.	n.s.	4.1	n.s.	n.s.
NO_3^{-}	W	2.4±1.0	3.3±1.0	4.2±1.5	4.9±2.4	5.8±2.0	3.8±1.3	3.9±1.3	1.5	0.3±1.1	n.s.	1.9±1.3	0.3±0.6
	C	1.4±0.4	2.5±0.9	3.2±2.9	0.7±0.7	2.7±0.7	0.1±0.1	2.4±0.4	n.s.	n.s.	0.2	n.s.	n.s.
Cl^{-}	W	3.2±0.2	3.6±0.4	5.1±0.7	5.2±2.7	4.7±0.8	4.5±0.9	4.2±0.8	17.6	6.1±1.1	n.s.	3.9±0.4	4±0.7
	C	7.7±1.6	5.7±1.89	5.2±0.6	5.2±0.4	5.0±0.3	4.9±0.3	5.1±0.4	n.s.	n.s.	106.4	n.s.	n.s.
HCO_3^{-}	W	103.1±12.7	131.4±37.3	238.4±16.4	270.6±43.0	254±44.5	243.8±24.9	250.9±73.0	237.5	294.3±25.7	n.s.	44.1±21.2	11.6±6.8
	C	105.7±4.4	192.3±68.4	240.9±7.6	212.1±32.5	302.5±50.8	282.4±14.7	250.2±9.0	n.s.	n.s.	833.6	n.s.	n.s.
Sr	W	0.2±0.0	0.2±0.1	0.6±0.1	0.5±0.1	0.5±0.1	0.4±0.1	0.4±0.1	0.3	0.3±0.0	n.s.	0.1±0.1	0.1±0.1
	C	0.1±0.0	0.5±0.3	0.5±0.2	0.2±0.1	0.5±0.1	0.3±0.1	0.4±0.1	n.s.	n.s.	2.7	n.s.	n.s.

Si	W	0.9±0.1	1.3±0.3	2.4±0.4	2.2±0.3	2.1±0.3	1.8±0.1	1.9±0.3	1.3	3.9±0.3	n.s.	4.4±2.9	2.7±1.9
	C	0.3±0.2	1.8±1.3	1.8±1.0	1.1±1.1	1.2±0.9	1.3±1.2	1.9±1.0	n.s.	n.s.	9.1	n.s.	n.s.
TDS	W	133.1±15.0	193.3±72.7	378.3±47.1	439.2±96.0	422.7±88.6	356.4±29.6	364±100.0	302.9	264.6±18.2	n.s.	81.8±47.9	29±18.6
	C	115.7±19.3	360.0±191.1	368.2±51.5	272.5±61.0	515.6±106.3	302.6±52.2	382.3±42.1	n.s.	n.s.	1059.4	n.s.	n.s.
DOC	W	0.7±0.2	0.7±0.2	0.7±0.2	4.6±7.1	3.0±4.3	2.2±3.0	2.3±7.1	n.s.	13.1±1.3	n.s.	0.4±0.1	1.2±1.3
	C	3.7±0.9	0.9±0.6	0.6±0.1	2.9±1.2	1.9±0.8	1.6±0.1	1.8±0.5	n.s.	n.s.	n.s.	n.s.	n.s.
DIC	W	16±2.1	21±7.5	38.7±6.3	48.2±10.3	43.1±6.3	39.8±4.9	43.1±13.7	n.d.	45.3±11.4	n.s.	6.9±3.2	4.1±3.3
	C	16.3±1.5	32.7±13.2	41.3±1.7	36.3±5.9	53±10.8	49±2.2	43±0.7	n.s.	n.s.	n.s.	n.s.	n.s.
$\delta^{18}O_{VSMOW}$ ‰	W	-8.5±0.5	-8.3±0.2	-8.4±0.1	-8.3±0.2	-8.4±0.2	-7.9±0.1	-7.9±0.2	-5.8474	-4.3±0.3	n.s.	-9±0.9	-12.8±3.7
	C	-9.4±0.2	-8.4±0.3	-8.4±0.2	-8.3±0.5	-8.2±0.1	-8.1±0.1	-7.8±0.0	n.s.	n.s.	-7.8	n.s.	n.s.
δD_{VSMOW} ‰	W	-47.7±4.5	-46.8 ±1.8	-48±1.2	-47.2±1.7	-48.1±1.8	-43.9±0.7	-43.7±1.7	-31.995	-24.1±1.7	n.s.	-50.8±8.11	-79.6±24.0
	C	-58.2±1.7	-48.4 ±1.8	-48.5±1.2	-47.3±2.7	-46.7±1.2	-45.6±0.9	-43.2±0.1	n.s.	n.s.	-47.9	n.s.	n.s.